

To be published in Journal of the Optical Society of America B:

Title: Formation mechanism of optical bistability in end-pumped quasi-three-level Tm, Ho:YLF lasers

Authors: Xinlu Zhang, LI li, and Yuezhu Wang

Accepted: 26 October 2009

Posted: 27 October 2009

Doc. ID: 115365

Formation mechanism of optical bistability in end-pumped quasi-three-level Tm, Ho:YLF lasers

Xinlu Zhang^{1,*}, Li Li¹, Yang Zheng¹, Yuezhu Wang²

¹ College of Science, Harbin Engineering University, Harbin, 150001, China

² National Key Laboratory of Tunable Laser Technology, Harbin Institute of Technology, Harbin, 150001, China

*Corresponding author: zhangxinlu1@yahoo.com.cn

We report on the optical bistability and its formation mechanism in an end-pumped quasi-three-level 2 μ m Tm,Ho:YLF laser with only a bulk laser crystal. We have experimentally observed that the characteristic output versus input curve is not linear and shows bistability, when the laser crystal is singly end-pumped by a 792nm laser diode. The width of the bistable region is 1.6W and the jump power at the turning point is 82.5mW. However, the laser shows linear output when the laser crystal is dual end-pumped. The formation mechanism of optical bistability is explained by solving the coupled rate equations in which the energy transfer upconversion and ground state reabsorption are considered. © 2007 Optical Society of America

OCIS codes: 140.3580, 140.3480, 140.5680.

1. INTRODUCTION

Optical bistability has many important applications in optical communications, optical logic, optical switch, cooling, and optical memory [1-5]. Generally, optical bistability systems fall into two categories: passive cavities containing either a saturable absorbing or a nonlinear dispersive medium, and laser systems with intracavity saturable absorbers [6]. To absorption bistability for

a laser system, optical bistability is usually associated with two-section structures where one section is actively pumped while the other acts as a saturable absorber [7]. If the saturation absorption intensity of the absorber is lower than the saturation intensity of the amplifier, the laser shows optical bistability. The dynamics of lasers containing an intracavity saturable absorber has been extensively studied during the last decade and optical bistability has been observed in many types of lasers [8-14]. But, until now, the formation mechanism of optical bistability in the quasi-three-level solid state lasers has not been clearly reported yet. It has been widely known that saturable reabsorption is one of the fundamental characteristics of (quasi-) three-level ion-doped mediums, but not all (quasi-) three-level lasers have the bistable characteristics [6]. Therefore, it is very meaningful to investigate the formation mechanism of optical bistability in (quasi-) three-level solid state lasers for various kinds of applications. We have experimental observed the phenomenon of bistable output in Tm,Ho:YLF lasers [9, 12]. In this paper, we investigate the formation mechanism of optical bistability in an end-pumped quasi-three-level Tm,Ho:YLF laser with only a bulk laser crystal, and without other saturable absorption materials in the cavity. The analytical expressions of the threshold pump powers, the width of bistable region, and the jump power at the on-threshold are obtained by solving the rate equations in which the energy transfer upconversion and ground state reabsorption are considered. Our investigation on the Tm,Ho:YLF bistable lasers can also be used to other kinds of (quasi)-three-level bistable lasers.

2. EXPERIMENTAL RESULTS

The plano-concave resonators were employed and the laser crystal was located inside the laser cavity, very close to the flat rear mirror. The Tm,Ho:YLF laser crystal has dopant concentrations of 6 at.% Tm³⁺ and 0.4 at.% Ho³⁺ with dimension of 4mm×4mm×10mm. The two faces were

antireflection coated at 2050nm and 792nm. To efficiently remove the generated heat during the experiment, the Tm,Ho:YLF crystal was wrapped with indium and mounted in a copper heat sink. The temperature of the copper heat sink was maintained at 253K with a thermoelectric cooler. The rear mirror was a plane dichroic mirror, having high reflection (HR) ($R > 99.8\%$) at 2050nm and high transmission (HT) ($T > 95\%$) at 792 nm pumping wavelength. The concave output coupler had a radius of curvature of 20cm. The crystal was end-pumped by output power 20W fiber-coupled laser diodes with the emission wavelength at 792nm. The diameter and numerical aperture of the fiber core were 400 μm and 0.22 respectively. Two lens of 50mm focal length to focus the pump beam. The pump spot radius in the position of the crystal was about 250 μm .

Figure 1 shows the output power as a function of the incident pump power with the 3% output coupler. Fig. 1 (a) is for the singly end-pumped configuration. When the pump power is increased from zero, the 2 μm laser does not oscillate until a critical point of pump power, referred to as on-threshold, is reached at $P_{in} = P_{th,on} = 4.3\text{W}$, at which the output power jumps from zero to a substantial level of 82.5mW. Above this point the output power increases nearly linearly with pump power. When the pump power is decreased starting from a level in excess of $P_{th,on}$, the output power decreases with the same slope, with the laser still oscillating for pump powers below $P_{th,on}$. Further reduction of the pump power eventually leads to cessation of the 2 μm laser oscillation at the off-threshold $P_{th,off} = 2.7\text{W}$. Therefore, in the pump power range defined by $P_{th,off} < P_{in} < P_{th,on}$, the operation of the Tm,Ho:YLF laser is bistable, and the output power at a given pump level depends on the way that this pump level is reached. Fig. 1 (b) is for the dual end-pumped configuration, and the pump power from the dual ends is synchronously

changed. It can be noted from Fig. 1 (b) that the output power is linear with the pump power and the optical bistability phenomenon disappears.

3. THEORETICAL ANALYSIS AND DISCUSSIONS

The energy level diagram for Tm,Ho:YLF lasers is shown in Fig. 2. The Tm^{3+} ions are excited to $^3\text{H}_4$ manifold by absorbing the 792nm pump light from the diode laser, and the $^3\text{F}_4$ manifold is efficiently populated through the well-known two-for-one cross-relaxation process. A fraction of the energy stored in the $\text{Tm}^{3+} ^3\text{F}_4$ manifold is then transferred to the $\text{Ho}^{3+} ^5\text{I}_7$ manifold. The $^5\text{I}_7$ long-lived metastable state acts as good population reservoir and allows a high density of excited ions to be created. As the populations of $^3\text{F}_4$ and $^5\text{I}_7$ grow, the long lifetimes ($\sim 10\text{ms}$) of the levels are reduced by the energy transfer upconversion (ETU) ($^3\text{F}_4 + ^5\text{I}_7 \rightarrow ^3\text{H}_6 + ^5\text{I}_5$). The ETU reduces the effective lifetime of the upper level $^5\text{I}_7$, and increases the threshold pump power of $2\mu\text{m}$ laser. The laser emission at $2\mu\text{m}$ is due to a transition between the lowest Stark level in the $^5\text{I}_7$ manifold and a high level in the $^5\text{I}_8$ ground state manifold. At near room temperature, the population density on the lower laser level is not presumed to be zero, so there is the ground state reabsorption (GSR) of $2\mu\text{m}$ laser in the $\text{Ho}^{3+} ^5\text{I}_8$ manifold.

The average transfer time between Tm^{3+} and Ho^{3+} manifolds is in the range of $10\mu\text{s}$ with normal dopant concentrations (4-6% Tm^{3+} , 0.5% Ho^{3+}), and is less than the lifetimes ($\sim 10\text{ms}$) of $\text{Ho}^{3+} ^5\text{I}_7$ and $\text{Tm}^{3+} ^3\text{F}_4$ manifolds, so, it is reasonable to treat $\text{Ho}^{3+} ^5\text{I}_7$ and $\text{Tm}^{3+} ^3\text{F}_4$ manifolds as a coupling upper state under continuous wave laser operating condition. Moreover, the lifetimes of the other upper levels (less than $30\mu\text{s}$) are sufficiently short compared with those of $\text{Ho}^{3+} ^5\text{I}_7$ and $\text{Tm}^{3+} ^3\text{F}_4$, and their populations can be neglected. Particularly, the deexcitation of $^3\text{H}_4$ is infinitely fast, therefore, the pump process is tantamount to a direct pumping from $^3\text{H}_6$ to $^3\text{F}_4$. To better explain the phenomenon of the optical bistability in end-pumped Tm,Ho:YLF lasers, with

the above approximations, we gave the quasi-three-level rate equations by taking into account the GSR and ETU effects as follows [15-17]:

$$N_2 = N_{Tm} - N_1 \quad (1)$$

$$N_4 = N_{Ho} - N_3 \quad (2)$$

$$N_2 + N_4 = (1 - f_{Ho})N_u + f_{Ho}N_u = N_u \quad (3)$$

$$\frac{dN_u}{dt} = \eta_p R r_p(r, z) - \frac{N_u}{\tau} - QN_u^2 - \frac{\sigma}{n} [f_{Ho}(f_u + f_l)N_u - f_l N_{Ho}] \Phi \phi_l(r, z) \quad (4)$$

where N_1 , N_2 , N_3 , and N_4 are the population densities of levels 3H_6 , 3F_4 , 5I_8 and 5I_7 respectively; N_u is the population density of the coupling upper state; N_{Ho} is the concentration of the doped Ho^{3+} population in the Tm, Ho:YLF crystal; c is the speed of light in vacuum; σ is the stimulated emission cross-section. For incident pump power P_{in} , pump rate R can be written as $R = \eta_\alpha P_{in} / h\nu_p$, where ν_p is the frequency of pump beam, h is the Planck's constant, $\eta_\alpha = 1 - \exp(-\alpha l)$ is the fraction of incident pump power absorbed in the crystal of length l with an absorption coefficient α ; $\Phi = 2l_{eff} P_{out} / ch\nu T$ is the cavity photon number, where P_{out} is the laser output power, ν is the frequency of output laser, T is the output coupler transmission at the laser wave length; $l_{eff} = l_{cav} + (n-1)l$ is the effective length of the resonator, l is the crystal length, n is the index of refraction at the laser wavelength; f_{Ho} represents the fractional population of Ho^{3+} ions in the coupling upper level, and it can be given by a boltzmann distribution [15]; η_p is the pump quantum efficiency to the Tm^{3+} 3F_4 manifold, which takes into account the cross relaxation effect and its competition with Tm^{3+} 3H_4 deexcitation channels; f_u and f_l are the fractions of the total 5I_7 and 5I_8 population density residing in laser upper level and lower level respectively, they are only dependent on temperature of the laser crystal and can be described by boltzmann statistics [16]; τ is the lifetime of the coupling upper state, and τ is given by [15]:

$$\frac{1}{\tau} = \frac{f_{Ho}}{\tau_{Ho}} + \frac{1-f_{Ho}}{\tau_{Tm}} \quad (5)$$

where, τ_{Ho} and τ_{Tm} are the intrinsic lifetimes of Ho 5I_7 and Tm 3F_4 manifolds. Q is the ETU coefficient and can be written as [15 , 17]:

$$Q = f_{Ho}(1-f_{Ho})(1-\frac{\eta}{2})q \quad (6)$$

where q is the rate constant for the ETU, and η is the quantum efficiency for the up-converted excitation to relax back to the Tm $^{3+}^3F_4$ and Ho $^{3+}^5I_7$ manifolds. We assume that the pump and laser beams are TEM₀₀ Gaussian distributions. For the singly end-pumped configuration, the normalized pump distribution is given by:

$$r_p(r, z) = \frac{2\alpha}{\eta_\alpha \pi \omega_p^2} \exp\left(-\frac{2r^2}{\omega_p^2}\right) \exp(-\alpha z) \quad (7)$$

where, ω_p is the average pump beam radius in the laser crystal, r is the transverse radial coordinate, and the normalized photon density in free space is given by:

$$\phi_l(r, z) = \frac{2}{\pi \omega_l^2 l_{eff}} \exp\left(-\frac{2r^2}{\omega_l^2}\right) \quad (8)$$

where, ω_l is the laser beam radius. Under the threshold condition of steady state, $dN_u/dt=0$, $\Phi=0$, and the general expression for N_u derived from Eqs. (1) - (4) is given by:

$$N_u = \frac{\eta_p R \tau_p(r, z)}{1 + Q \tau^2 R \eta_p r_p(r, z)} \quad (9)$$

The condition that the population inversion is realized under the threshold pump power is then written as:

$$\Delta N = f_u N_4 - f_l N_3 = \int f_{Ho} N_u - f_l N_{Ho} \geq 0 \quad (10)$$

where, $f = f_l + f_u$. From Eqs. (7)-(10) the population inversion region can be solved as:

$$r \leq \left\{ \frac{\omega_p^2}{2} \left[\ln \frac{2\alpha(ff_{Ho} - Qf_l N_{Ho} \tau) \tau \eta_p P_{in}}{\pi f_l N_{Ho} \omega_p^2 h \nu_p} - \alpha z \right] \right\}^{\frac{1}{2}} \quad (11)$$

With the Eq. (11) and the following parameters: $\lambda_p=792\text{nm}$, $\alpha=5.4\text{cm}^{-1}$ [18], $\eta_p=1.57$ [19], $f_u=0.092$ [20], $f_l=0.019$ [20], $f_{Ho}=0.65$ [20], $\eta=1$ [15], $q=4 \times 10^{-17} \text{cm}^3/\text{s}$ [21], $\tau_{Tm}=8\text{ms}$ [16], $\tau_{Ho}=18\text{ms}$ [16], $N_{Ho}=5.59 \times 10^{19} \text{cm}^{-3}$, $l=10\text{mm}$, $\omega_p=250\mu\text{m}$, we calculate the population inversion region for five different pump powers as shown in Fig. 3. It can be noted from Fig. 3 that when the on-threshold pump power $P_{on, th}$ is equal to 4.3W, the rear half part of the crystal is in the non-inversion region, and it can be regarded as a saturable absorber due to GSR of the Tm,Ho:YLF laser crystal.

From Eq. (4), the effective coupling upper level lifetime can be defined in the following form:

$$\frac{1}{\tau_{eff}} = \frac{1}{\tau} + QN_u = \frac{QN_u \tau + 1}{\tau} \quad (12)$$

Substituting Eqs (7) and (9) into Eq (12), the equation clearly describing the influence of ETU on the effective coupling upper level lifetime along crystal center-axis can be written as:

$$\tau_{eff} = \tau \frac{\pi \omega_p^2 h \nu_p + 2Q\alpha \eta_p \tau^2 P_{in} \exp(-\alpha z)}{\pi \omega_p^2 h \nu_p + 4Q\alpha \eta_p \tau^2 P_{in} \exp(-\alpha z)} \quad (13)$$

Equation (13) clearly shows that the ETU effect reduces the effective lifetime of the coupling upper level. At the on-threshold pump power of 4.3W, the effective lifetime of the coupling upper level along the laser crystal center-axis for the singly end-pumped configuration is shown as Fig. 4. It can be seen from Fig. 4, the effective lifetime near the pumped end is lower than that far from the pumped end, because the influence of ETU effect gets more severe with the increase of population density in upper level. The gain region (the fore half part of crystal whose length

is l_g) has a shorter upper level effective lifetime than the absorbing region (the rear half part of crystal whose length is l_a) at on-threshold pump power, so the gain region has a larger saturation absorption intensity than the absorbing region, and the Tm,Ho:YLF laser for the singly end-pumped configuration satisfies the condition of optical bistability [13].

For the singly end-pumped configuration, the saturation intensity $I_{s,g}$ of the gain region and the saturation intensity $I_{s,a}$ of the absorption region can be respectively written as:

$$I_{s,g} = h\nu/2(f_u + f_l)\sigma\tau_g, \quad I_{s,a} = h\nu/2(f_u + f_l)\sigma\tau_a \quad (14)$$

where τ_g and τ_a are the effective upper level lifetimes in the gain region and the absorption region respectively, and ν is the frequency of output laser. We can see from Fig. 4 that the effective upper level lifetime τ_a in the absorption region is longer than the effective upper level lifetime τ_g in the gain region. So the saturation intensity $I_{s,g}$ of the gain region is more than the saturation intensity $I_{s,a}$ of the absorption region, and the absorption region is easier to be saturated than the gain region. When the laser does not oscillate, the intracavity light intensity I is nearly equal to zero, and the absorber is in its unbleached state. Once the pump power increases to the on-threshold pump power, the pump would lift the gain to the unsaturated value of the losses. The gain under the condition of on-threshold pump power is equal to the unsaturation losses because the absorption is in its unbleached state, and it can be expressed as [22]:

$$G_{th,on} = \delta_{on} = 2f_l\sigma N_{Ho}l_a + (L + T) \quad (15)$$

where, L is the intracavity loss, T is the transmittance of the output coupler, l_a is the length of absorption region. Under the condition of on-threshold pump power, the intracavity power grows slowly, starting from spontaneous emission noise, until the intracavity intensity is enough to bleach the saturation absorber (the absorption region). The absorption region saturates before the gain region begins to saturate, because the saturation intensity $I_{s,g}$ of the gain region is more than

the saturation intensity $I_{s,a}$ of the absorption region. Then, the intracavity power increases quickly until the net gain is equal zero. We can find that once the laser begins to oscillate, the saturation of absorption is faster than that of gain, so the output power of the laser has a big jump at the on-threshold pump power.

When the pump power decreases from a value over on-threshold pump power, and the laser is in oscillating state, the absorption of the absorption region is saturated, the gain under the condition of off-threshold pump power is equal to the saturation losses, and can be approximately obtained as [22]:

$$G_{th,off} = \delta_{off} \approx (L+T) \quad (16)$$

From Eqs (15) and (16), it can be noted that $G_{th,on}$ is larger than $G_{th,off}$, and there are two output power values at the same pump power between $G_{th,off}$ and $G_{th,on}$.

The condition for threshold is that the round trip gain averaged over the cavity mode equals the round trip loss, and this threshold condition can be written as:

$$G = 2\sigma_{eff} \int_{l_g} \Delta N \cdot \phi_l(r, z) dV = \delta \quad (17)$$

Where, δ is the round trip loss under the threshold condition. Substituting Eq. (9) into Eq. (10), the steady state inversion population density can be obtained as:

$$\Delta N = \frac{\eta_p R_{ff} \tau_p(r, z)}{1 + Q\tau^2 R \eta_p r_p(r, z)} - f_l N_{Ho} \quad (18)$$

Substituting Eqs. (7), (8) and (18) into Eq. (17), and the threshold pump power of Tm,Ho:YLF lasers can be obtained as:

$$P_{th} = P_{th0}(1 + \beta) \quad (19)$$

In Eqs. (19) parameters P_{th0} and β are defined as follows:

$$P_{th0} = \frac{nh\nu_p}{2\tau\eta_p\eta_\alpha ff_{Ho}l_{eff}\sigma} (\delta + \delta_{l_g}) \frac{1}{\int_{l_g} \phi_l r_p dV} \quad (20)$$

$$\beta = \frac{Q\tau^2\eta_p\eta_\alpha P_{th0}}{h\nu_p} \frac{\int_{l_g} \phi_l r_p^2 dV}{\int_{l_g} \phi_l r_p dV} \quad (21)$$

Here, P_{th0} is the threshold pump power without the ETU effect. Equation (19) indicates that the ETU increases the threshold pump power by the factor $(1+\beta)$, furthermore, the influence of the ETU to the threshold pump power P_{th} depends on the threshold pump power P_{th0} and increases with the increase of the whole loss. In addition, the dependence of the β parameter on the spatial variation of both the pump beam and the cavity field can be explicitly expressed in Eq. (21). Because Tm,Ho:YLF laser is the quasi-three-level system, additional term δ_{l_g} appears in Eq. (20). δ_{l_g} is the loss term of gain region that is due to the population in the lower laser level and can be given by:

$$\delta_{l_g} = \frac{2f_l N_{Ho} \sigma_{l_{eff}}}{n} \int_{l_g} \phi_l dV = 2f_l N_{Ho} \sigma_{l_g} \quad (22)$$

For the on-threshold, the cavity loss $\delta = \delta_{on}$, and substituting Eqs. (15) and (22) into Eq. (20), the analytical expressions for the on-threshold pump power can be obtained as:

$$P_{th,on} = P_{th0,on} (1 + \beta_{on}) \quad (23a)$$

$$P_{th0,on} = \frac{nh\nu_p}{2\tau\eta_p\eta_\alpha ff_{Ho}l_{eff}\sigma} (L + T + 2f_l \sigma N_{Ho} l) \frac{1}{\int_{l_g} \phi_l r_p dV} \quad (23b)$$

$$\beta_{on} = \frac{Q\tau^2\eta_p\eta_\alpha P_{th0,on}}{h\nu_p} \frac{\int_{l_g} \phi_l r_p^2 dV}{\int_{l_g} \phi_l r_p dV} \quad (23c)$$

For the off-threshold, the cavity loss $\delta = \delta_{off}$, and substituting Eqs. (16) and (22) into Eq. (20), the analytical expressions for the off-threshold pump power can be obtained as:

$$P_{th,off} = P_{th0,off} (1 + \beta_{off}) \quad (24a)$$

$$P_{th0,off} = \frac{nh\nu_p}{2\tau\eta_p\eta_\alpha f_{Ho} l_{eff} \sigma} (L + T + 2f_l \sigma N_{Ho} l_g) \frac{1}{\int_{l_g} \phi_l r_p dV} \quad (24b)$$

$$\beta_{off} = \frac{Q\tau^2\eta_p\eta_\alpha P_{th0,off} \int_{l_g} \phi_l r_p^2 dV}{h\nu_p \int_{l_g} \phi_l r_p dV} \quad (24c)$$

So, the width of bistable region can be written as

$$\Delta P_{th} = P_{th,on} - P_{th,off} \quad (25)$$

At the range of bistable region, the laser has two output powers. The output power corresponds to the high value when the pump power decreases to a certain value from a value over the on-threshold pump power. Reversely, the output power corresponds to the low value when the pump power increases to the value from zero.

For the quasi-three-level laser systems far above threshold, the slope efficiency approaches to that of a four-level laser, so the slope efficiency for Tm,Ho:YLF laser is give by [15]:

$$\eta = \eta_p \frac{\lambda_p}{\lambda} \frac{T}{L+T} \quad (26)$$

where λ is the output wavelength, λ_p is the pump wavelength. Equation (26) explicitly indicates that the slope efficiency is only dependent on the loss when the output coupling is determined. So it can be noted from Fig. 1 that the Tm,Ho:YLF laser has same slope values at different pump powers when the laser keeps oscillating state. Furthermore, when the pump power increases to the on-threshold pump power and the laser begins to oscillate, the saturable absorption of the absorption region is bleached immediately [23], so the output power of 2 μ m laser shows a big

jump value. When the laser keeps oscillating state, the output power can be approximately expressed as:

$$P_{out} = \eta_p \frac{\lambda_p}{\lambda} \frac{T}{L+T} (P_{in} - P_{th,off}) \quad (27)$$

With Eqs. (23), (24), (27), and the following parameters: $\lambda_p=792\text{nm}$, $\lambda=2.06\mu\text{m}$, $\alpha=5.4\text{cm}^{-1}$ [18], $\eta_p=1.57$ [19], $f_u=0.092$ [20], $f_l=0.019$ [20], $f_{Ho}=0.65$ [20], $q=4\times 10^{-17}\text{cm}^3/\text{s}$ [21], $\tau_{Tm}=8\text{ms}$ [16], $\tau_{Ho}=18\text{ms}$ [16], $\eta=1$ [15], $N_{Ho}=5.59\times 10^{19}\text{cm}^{-3}$, $l=10\text{mm}$, $\omega_p=250\mu\text{m}$, $l_a=l_g=5\text{mm}$, $T=0.03$, and $L=0.1$, we calculate the input-output power characteristics of the singly end-pumped Tm,Ho:YLF laser as shown in Fig. 5. It can be noted that the theoretical results in Fig. 5 and the experimental results in Fig. 1(a) have similar variation curve, so the present theoretical analysis is confirmed to be reasonable.

For the dual end-pumped configuration, the normalized pump distribution is given by:

$$r_p(r, z) = \frac{2\alpha}{\eta_a \pi \omega_p^2} \exp\left(\frac{-2r^2}{\omega_p^2}\right) \{\exp(-\alpha z) + \exp[-\alpha(l-z)]\} \quad (28)$$

Substituting Eqs. (9) and (28) into Eq. (10), the population inversion region for the dual end-pumped configuration can be solved as:

$$r \leq \frac{\omega_p}{\sqrt{2}} \left\{ \ln \frac{2\alpha(ff_{Ho} - Qf_l N_{Ho} \tau) \tau \eta_p P_{in} [\exp(-\alpha z) + \exp(\alpha z - \alpha l)]}{\pi f_l N_{Ho} \omega_p^2 h \nu_p} \right\}^{\frac{1}{2}} \quad (29)$$

We can obtain the population inversion region for the double end-pumped configuration at five different pump powers as shown in Fig. 6. It can be noted from Fig. 6 that when the threshold pump power is equal to 2W, the crystal along the whole length is in the population inversion region, and the absorption region does not exist any more, so the optical bistability phenomenon is absent as shown in Fig. 1 (b).

4. CONCLUSIONS

We studied the mechanism of optical bistability in a laser diode end-pumped Tm,Ho:YLF laser at $2\mu\text{m}$ with only a bulk laser crystal. When the laser crystal is singly end-pumped, the width of the bistable region is 1.6W, and the jump power at the turning point is 82.5mW for the transmittance of 3%. The optical bistability behavior of Tm,Ho:YLF laser was analyzed theoretically based on the quasi-three-level rate equation theory. When the laser crystal is single-end-pumped, the distribution of pump power is non-uniform along the axis of the crystal. The laser crystal absorbs in the low pump intensity region due to the ground state reabsorption effect, and in the high pump intensity region the laser crystal amplifies. At the same time, the reduction of the effective upper level lifetime is more severe in gain region than in absorption region, and there is a larger saturation intensity in the absorption than in gain region. So the bistable output of $2\mu\text{m}$ laser mainly results from the nonlinear saturation of the ground state reabsorption in absorption region and the energy transfer upconversion effects. The theoretical analysis is generally applicable to other kinds of (quasi)-three-level bistable lasers.

ACKNOWLEDGEMENTS

The authors acknowledge support of the Doctoral Program Foundation of Institution of Higher Education of China (grant no 20070217014) and the National Nature Science Foundation of China (grant nos 60878016 and 10804022) and Natural Science foundation of Heilongjiang Province (grant no A200801) and the Innovation Talents Foundation of Harbin City (grant no 2008RFQXG026).

REFERENCES

1. D. A. Mazurenko, R. Kerst, and J. I. Dijkhuis, "Ultrafast optical switching in three dimensional photonic crystals," *Phys. Rev. Lett.* **91**, 213903 (2003).
2. L. D. Bozano, B. W. Kean, V. R. Deline, J. R. Salem, and J. C. Scott, "Mechanism for bistability in organic memory elements," *Appl. Phys. Lett.* **84**, 607-609 (2004).
3. M.Y. Vilensky, Y. Prior, and I. S. Averbukh, "Cooling in a bistable optical cavity," *Phys. Rev. Lett.* **99**, 103002 (2007).
4. F. Y. Wang, G. X. Li, H. L. Tam, K. W. Cheah, and S. N. Zhu, "Optical bistability and multistability in one-dimensional periodic metal-dielectric photonic crystal," *Appl. Phys. Lett.*, **92**, 211109 (2008).
5. E. Weidner, S. Combrié, A. De Rossi, O.-V. Tran, and S. Cassette, "Nonlinear and bistable behavior of an ultrahigh-Q GaAs photonic crystal nanocavity," *Appl. Phys. Lett.*, **90**, 101118 (2007).
6. J. Liu, V. Petrov, U. Griebner, F. Noack, H. Zhang, J. Wang, and M. Jiang, "Optical bistability in the operation of a continuous-wave diode-pumped Yb:LuVO₄ laser," *Opt. Express*. **14**, 12183-12187 (2006).
7. X. D. Huang, A. Stintz, H. Li, A. Rice, and G. T. Liu, "Bistable operation of a two-section 1.3 μ m InAs quantum dot laser-absorption saturation and the quantum confined stark effect," *IEEE J. Quantum Electron.* **37**, 414-417 (2001).
8. O. Qasaimeh, W.D. Zhou, J. Philips, G. T. Liu, J. Cheng, and K. J. Malloy, "Bistability and self-pulsation in quantum-dot lasers with intracavity quantum-dot saturable absorbers," *Appl. Phys. Lett.*, **74**, 1654-1656 (1999).
9. X. Zhang and Y. Wang, "Optical bistability effects in a Tm,Ho:YLF laser at room temperature," *Opt. Lett.* **32**, 2333-1335 (2007).

10. Q. H. Mao and J. W. Y. Lit, "Widely tunable L-band erbium-doped fiber laser with fiber bragg gratings based on optical bistability," *Appl. Phys. Lett.* **82**, 1335-1337 (2003).
11. S. Ishii and T. Baba, "Bistable lasing in twin microdisk photonic molecules," *Appl. Phys. Lett.* **87**, 1811021 (2005).
12. X. Zhang, Y. Wang, L. Li, Y. Ju, J. Cui, and Y. Lv, "End-Pumped Optical Bistability Tm,Ho:YLF Laser," *Laser Physics.* **19**, 392-395 (2009).
13. Y. Mitnick, M. Horowitz, and B. Fischer, "Bistability in cavities with erbium-doped fiber amplifiers due to bidirectional pump-beam interference," *J. Opt. Soc. Am. B.* **14**, 2079-2082 (1997).
14. E. Arimondo, and B. M. Dinelli, "Optical bistability of a CO₂ laser with intracavity saturable absorber: Experiment and model," *Opt. Commun.* **44**(4), 277-282 (1983).
15. T. Y. Fan, G. Huber, R. L. Byre, and P. Mitzscherlich, "Spectroscopy and diode laser-pumped operation of Tm,Ho:YAG," *IEEE J. Quantum Electron.* **24**, 924-933 (1988).
16. D. Bruneau, S. Delmonte, and J. Pelon, "Modeling of Tm,Ho:YAG and Tm,Ho:YLF 2- μ m lasers and calculation of extractable energies," *Appl. Opt.* **37**, 8406-8419 (1998).
17. G. Rustad, and K. Stenersen, "Modeling of laser-pumped Tm and Ho lasers accounting for upconversion and ground-state depletion," *IEEE J. Quantum Electron.* **32**, 1645-1655 (1996).
18. G. L. Bourdet, and G. Lescroart, "Theoretical modeling and design of a Tm, Ho:YLiF₄ microchip laser," *Appl. Opt.* **38**, 3275-3281 (1999).
19. B. T. McGuckin, and R. T. Menzies, "Efficient CW diode-pumped Tm,Ho:YLF laser with tenability near 2.067 μ m," *IEEE J. Quantum Electron.* **28**, 1025-1028 (1992).
20. M. E. Storm, "Holmium YLF amplifier performance and the prospects for multi-joule energies using diode-laser pumping," *IEEE J. Quantum Electron.* **29**, 440-451 (1993).

21. G. Armagan, B. M. Walsh, N. P. Barnes, E. A. Modlin, and A. M. Buoncristiani, "Determination of Tm-Ho Rate Coefficients from Spectroscopic Measurements," in *Advanced Solid State Lasers*, T. Fan and B. Chai, eds., Vol. 20 of OSA Proceedings Series (Optical Society of America, 1994), pp:141-145
22. G. J. Spühler, R. Paschotta, R. Fluck, B. Braun, M. Moser, G. Zhang, E. Gini, and U. Keller, "Experimentally confirmed design guidelines for passively Q-switched microchip lasers using semiconductor saturable absorbers," *J. Opt. Soc. Am. B.* **16**, 376-388 (1999).
23. Y. Kuang, and Y. Chang, "Numerical study of passive Q switching of a Tm:YAG laser with a Ho:YLF solid-state saturable absorber," *Appl. Opt.* **42**, 1685-1691 (2003).

Published by
OSA

List of Figure Captions:

Fig. 1. The input-output power characteristics of end-pumped Tm,Ho:YLF lasers (a) the singly end-pumped configuration (b) the dual end-pumped configuration.

Fig. 2. Schematic of the major excitation and relaxation processes in Tm,Ho:YLF laser: CR, cross-relaxation; ET, energy transfer; ETU, energy transfer upconversion.

Fig. 3. The calculated population inversion region at different pump powers for the singly end-pumped configuration.

Fig. 4. The effective coupling upper level lifetime along the laser crystal center-axis at the on-threshold pump power of 4.3W.

Fig. 5. The calculated input-output power characteristics of the singly end-pumped Tm,Ho:YLF laser.

Fig. 6. The calculated population inversion region at different pump powers for the dual end-pumped configuration.

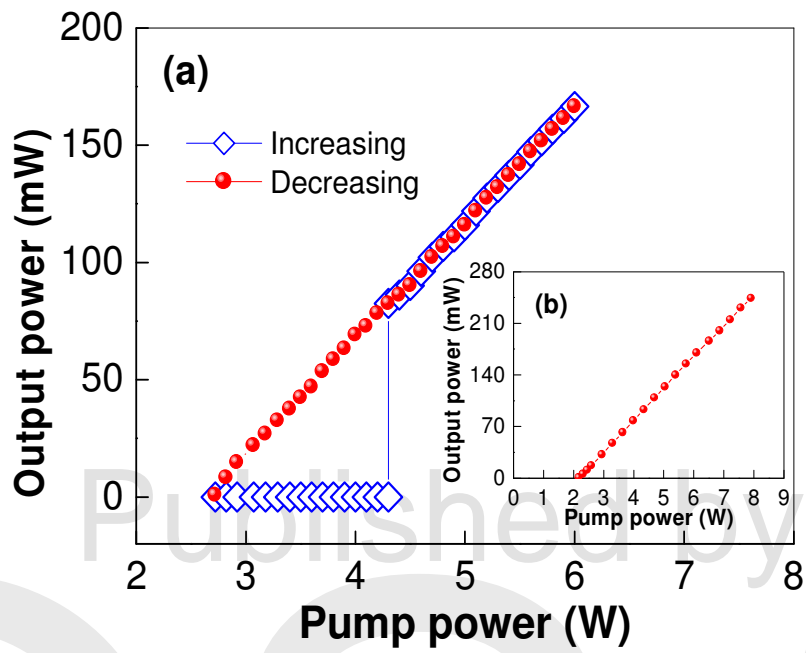


Fig. 1. The input-output power characteristics of end-pumped Tm,Ho:YLF lasers.

(a) the singly end-pumped configuration (b) the dual end-pumped configuration.

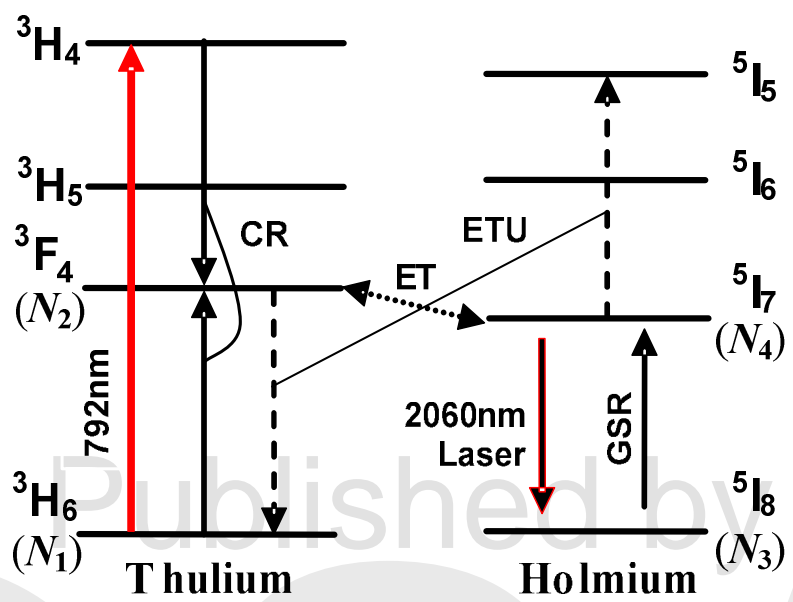


Fig. 2. Schematic of the major excitation and relaxation processes in Tm,Ho:YLF laser:

CR, cross-relaxation; ET, energy transfer; ETU, energy transfer upconversion, GSR, ground state reabsorption.

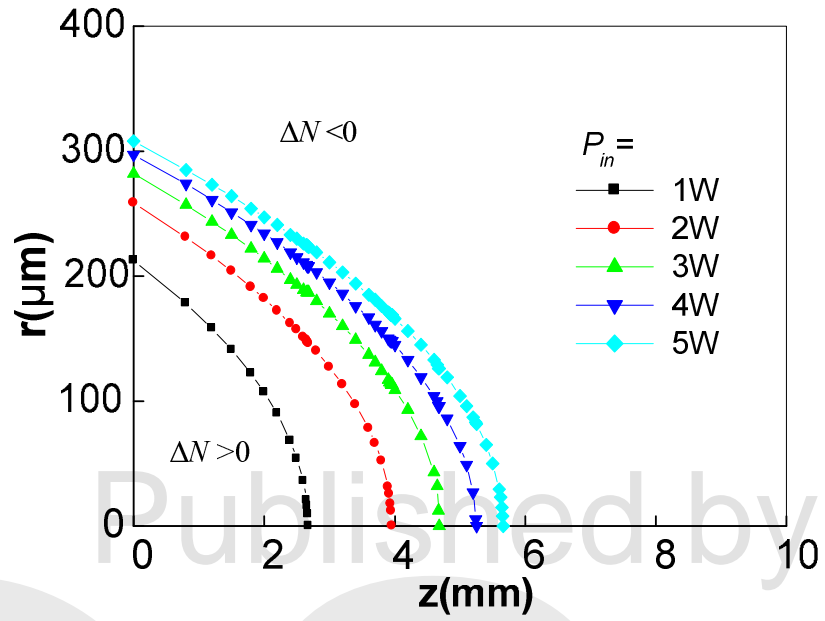


Fig. 3. The calculated population inversion region at different pump powers for the singly end-pumped configuration.

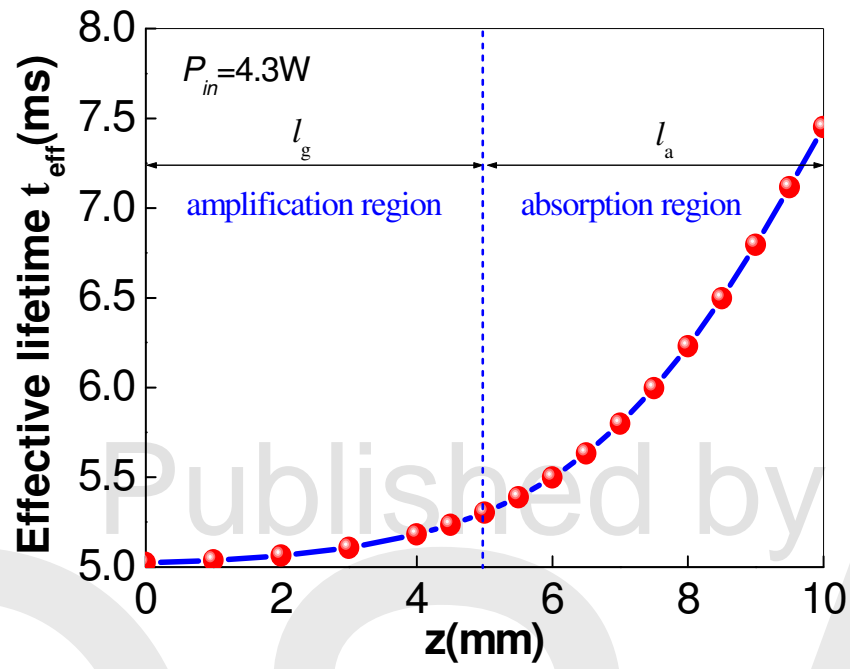


Fig. 4. The effective coupling upper level lifetime along the laser crystal center-axis at the on-threshold pump power of 4.3W.

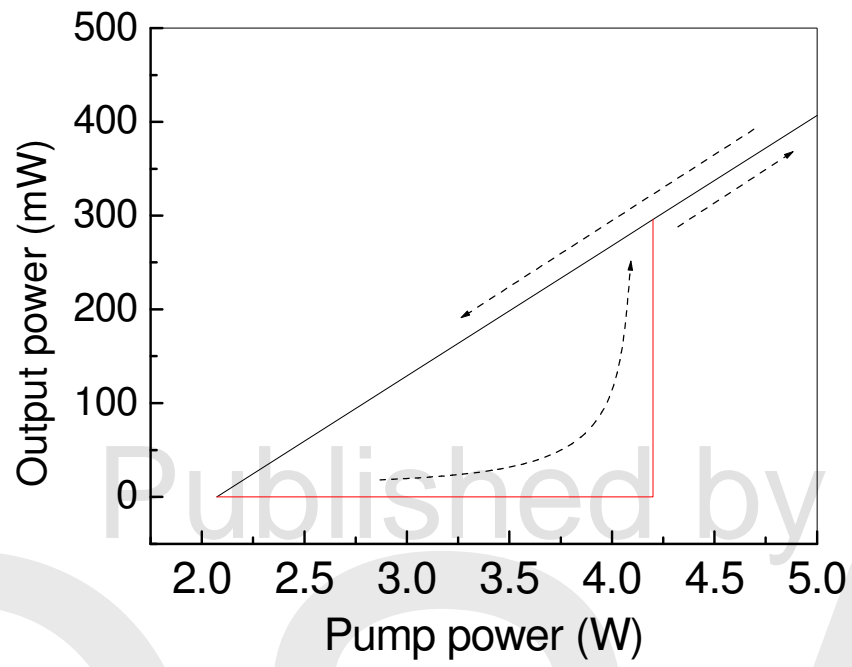


Fig. 5. The calculated input-output power characteristics of the singly end-pumped Tm,Ho:YLF laser.

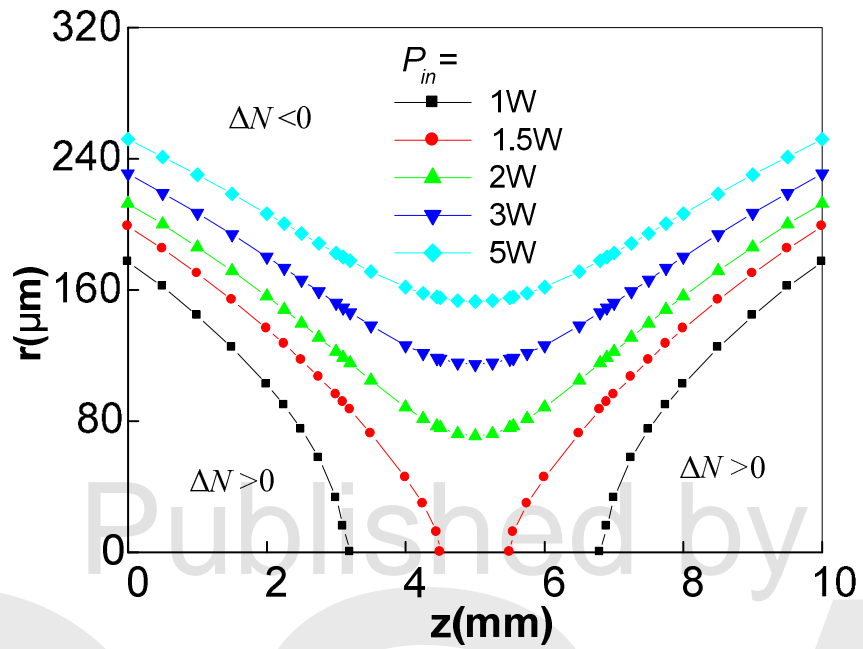


Fig. 6. The calculated population inversion region at different pump powers for the dual end-pumped configuration.